

# EFFECT OF CLOUDS ON SO<sub>2</sub> CHEMISTRY: A COMBINATION OF SATELLITE MEASUREMENTS AND TRAJECTORY MODELING

Marloes Penning de Vries\*, Steffen Beirle, Christoph Brühl, Steffen Dörner, Christoph Hörmann, Viktoria Keicher, Vinod Kumar, Andrea Pozzer, Holger Sihler, Simon Warnach, and Thomas Wagner

Max Planck Institute for Chemistry, Mainz, Germany

\*Now at: Deutscher Wetterdienst, Offenbach, Germany

## Abstract

The Kilauea volcano (Hawaii), currently one of the most active volcanos on Earth, has been continuously erupting since the beginning of 1983. A pronounced degassing phase in March–November 2008 caused the formation of an extensive SO<sub>2</sub> plume, which in turn led to the formation of sulfate aerosols. The steady trade winds and lack of interfering sources previously allowed us to determine the lifetime of SO<sub>2</sub> from satellite-based measurements. Additionally, indications were found that SO<sub>2</sub> is oxidized more rapidly in the presence of clouds. The current investigation was aimed at quantifying the effect of clouds on the SO<sub>2</sub> oxidation rate. Trajectory calculations using the HYSPLIT model were combined with hourly GOES cloud data to reconstruct a “cloud history” of OMI pixels displaying enhanced levels of SO<sub>2</sub>. The SO<sub>2</sub> data were subsequently sorted by the amount of clouds encountered since emission from the volcano. Thus obtained mean maps of SO<sub>2</sub> data with no cloud encounters were compared to maps of SO<sub>2</sub> data affected by clouds and significant differences were found which could, however, not be quantified.

## 1. INTRODUCTION

The comparison of global circulation models (GCMs) with observed data is essential for the evaluation and resulting improvement of GCMs. An ideal case for the evaluation of aerosol model data presented itself in 2008, when Kilauea, a volcano on the remote Hawaii Island, exhibited more than 8 months of continuous, strong degassing. The sustained high emissions of SO<sub>2</sub> caused a sulfate plume to form of at least 1500 km length. In the course of a model evaluation focusing on Kilauea’s sulfate aerosols it occurred to us that an important aspect of such a study is the consideration of the various effects of clouds, as they affect modeled and observed data in different ways. The effects can be roughly divided into those affecting satellite observations and those affecting SO<sub>2</sub> and aerosol physics and chemistry. The former depend on the optical properties of the cloud and its altitude with respect to the atmospheric component of interest, in our case: SO<sub>2</sub>. An optically thick cloud above an SO<sub>2</sub> plume, for example, will shield the layer from view from the satellite above, whereas a cloud below may enhance the sensitivity of the satellite instrument to the overlying plume. These effects can be well simulated using a radiative transfer model if both the cloud field and SO<sub>2</sub> profile are sufficiently well known. Needless to say, these effects play no role for modeled data – in contrast to the chemical effects and scavenging.

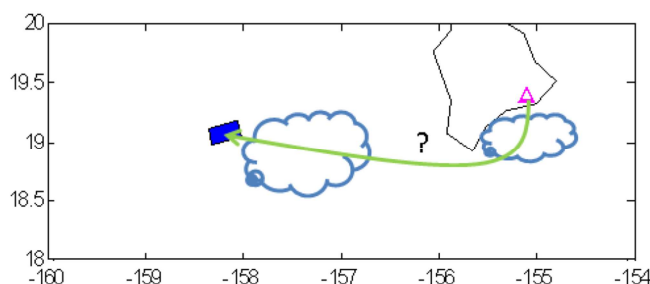


**Figure 1:** Schematic of the strategy of determining the “cloud history” of an air parcel at a given satellite pixel (blue rectangle). The cloud field at each point (t,x,y,z) along the air parcel’s trajectory (green arrow), starting at the volcano (pink triangle) is summed to obtain an estimate of the total amount of clouds encountered by the air parcel.

The current study is focused on the physico-chemical effects of clouds. Given that the oxidation rate of SO<sub>2</sub> is much higher under aqueous than under dry conditions, the lifetime of SO<sub>2</sub> should be much smaller in the presence of clouds. Indeed, an indication of this effect was found in a satellite-based study of SO<sub>2</sub> lifetime [Beirle et al., 2014]. To identify and, possibly, quantify this effect, we developed methods aimed at determining the “cloud history” of SO<sub>2</sub>-containing air parcels detected by satellite: in other words, the amount of clouds encountered by an air parcel since its emergence from the source, as schematically depicted in Fig. 1.

More specifically, we used satellite observations to determine the location of the SO<sub>2</sub> plume. For each satellite pixel, we determined the most probable trajectory from each satellite pixel back to the volcano (green arrow in Fig.1). Subsequently, we collected cloud data at each hourly step along the trajectory. By separating the SO<sub>2</sub> pixels based on their “cloud history”, the cloud effect should become apparent: an SO<sub>2</sub> mean map of all pixels with few cloud encounters should show a slower decay (longer SO<sub>2</sub> plume) than one in which pixels had a lot of interaction with clouds. We tried several methods of ever-increasing complexity, which will be briefly described in Section 3. In Section 2, the used data and model settings are given, Section 4 contains a description of our results, and Section 5 finalizes with some concluding remarks.

## 2. SATELLITE DATA AND MODELS

The results presented here were obtained using SO<sub>2</sub> data detected by OMI, the Ozone Monitoring Instrument [Levelt et al., 2006]. OMI is a spectrometer on NASA's Aura satellite, which flies in a polar orbit crossing the equator at about 13:30 local time. OMI has a spatial resolution of 13x24 km<sup>2</sup> at the center of its swath and achieved daily global coverage until the first occurrence in June 2007 of the so-called row anomaly, an instrumental problem that causes grievous radiance errors in up to half of the OMI ground pixels (see <http://projects.knmi.nl/omi/research/product/rowanomaly-background.php>). The row anomaly strongly affects the reliability of observations; therefore all affected pixels were removed from the data set prior to analysis. SO<sub>2</sub> data were analyzed as described in [Hörmann et al., 2013]; Slant Column Densities were transformed to Vertical Column Densities (VCDs) by assuming a geometrical air-mass factor. OMI pixels in which the cloud fraction was larger than 0.2, which adversely affects the SO<sub>2</sub> retrieval quality, were discarded. Pixels at OMI's swath edges, with widths exceeding 40 km, were also removed prior to analysis.

The cloud data used for the cloud history determination were hourly data from the IMAGER instrument on the geostationary GOES-11 satellite [Minnis et al., 2008], downloaded from [https://eosweb.larc.nasa.gov/project/ceres/geo\\_table](https://eosweb.larc.nasa.gov/project/ceres/geo_table). The GOES cloud optical thickness (COT) retrieval is very similar to the MODIS retrieval and both are in good agreement in most cases [Minnis et al., 2011]. Hawaii, however, is located at the western edge of GOES's field of view and is therefore viewed under a large angle. This strongly affects the retrieval quality, particularly when the sun is low. In addition, the visible channels cannot be used for cloud detection at night and the COT is estimated rather than retrieved. In the cloud-history analysis, GOES data around twilight were discarded, but no correction was applied for the difference between daytime and nighttime data.

The model data used in this study resulted from two dedicated runs of the ECHAM/MESSy Atmospheric Chemistry (EMAC) modular global climate and online coupled chemistry simulation system with aerosol sub-models for calculation of processes in the troposphere and middle atmosphere [Jöckel et al., 2010]. The simulation set-up was similar to that in [Pozzer et al., 2015]: MESSy version 2.50 was run with T63L31 resolution (1.9°x1.9°; 31 vertical levels below about 30 km); the meteorology was nudged to ECMWF analysis data. The emission of SO<sub>2</sub> by Kilauea was set to 21 Tg/day in July and 18 Tg/day in August (from GOME-2 emission estimates in [Beirle et al., 2014]), emitted in the box nearest to the volcano at 1.7 km altitude. Two identical simulations were run, in which the only difference was the switching off of SO<sub>2</sub> and sulfate scavenging by clouds. The model was run starting on July 1, 2008 and calculated up to August 31, 2008. For the analysis we only used data from August, regarding July as a spin-up month.

To reconstruct air parcel trajectories back to their volcanic source, we used the National Oceanic and Atmospheric Administration (NOAA) hybrid single-particle Lagrangian integrated trajectory HYSPLIT model [Draxler and Hess, 1998; Stein et al., 2015]. An unregistered version of HYSPLIT 4 (released in February 2016) was downloaded from [www.ready.noaa.gov/HYSPLIT.php](http://www.ready.noaa.gov/HYSPLIT.php). NOAA Global Data Assimilation System, GDAS [Kleist et al., 2009], data at 0.5° resolution were used as meteorological input for HYSPLIT.

### 3. INVESTIGATION OF CLOUD EFFECTS ON SO<sub>2</sub> OXIDATION

To reconstruct air parcel history, we connected the center of each satellite pixel with the volcano. Initially, a linear trajectory was assumed from pixel to volcano, but this method was soon abandoned in favor of more accurate trajectories calculated using the HYSPLIT trajectory model. In a second approach, trajectories were calculated up to 36 hours backwards to the volcano using the centers of OMI pixels as starting points, but that yielded many false positives (trajectories of SO<sub>2</sub>-free pixels leading back to the source), and many misses (SO<sub>2</sub>-containing pixels not reaching the source). In addition, inconsistent trajectories for neighboring pixels were found. The most accurate and consistent method we developed was based on HYSPLIT forward trajectories that started at the volcano. A large number of forward trajectory calculations were started at (or near) the source at altitudes between 0.5 and 2 km. Trajectories with an appropriate length were started at every hour for 36 hours before satellite overpass. For example: for OMI's overpass time of 23 UTC, a trajectory with length 1 hour was started at 22 UTC, one with length 2 hours at 21 UTC, and so forth, until finally with length 36 hours at 11 UTC on the previous day. The endpoints of these trajectory calculations are shown in the left panels of Fig. 2 for an orbit on Aug.7, 2008, at three different starting altitudes. The pattern of trajectories at each starting altitude was compared with the observed pattern of SO<sub>2</sub> (shown in gray in Fig. 2) by comparing three scores. The first, (shown in blue in the right panel of Fig. 2) is simply the fraction of interest; "successful" pixels being those OMI pixels that fall within a range of 0.1° of the trajectory endpoints. As this score is not selective for plume pixels, two more scores were determined: the fraction of "successful" pixels with SO<sub>2</sub> VCD > 1 DU and the ratio of the summed SO<sub>2</sub> VCDs of the "successful" pixels to the summed SO<sub>2</sub> VCDs of all OMI pixels within the region of interest (green and red lines in the right panel of Fig.2, respectively).

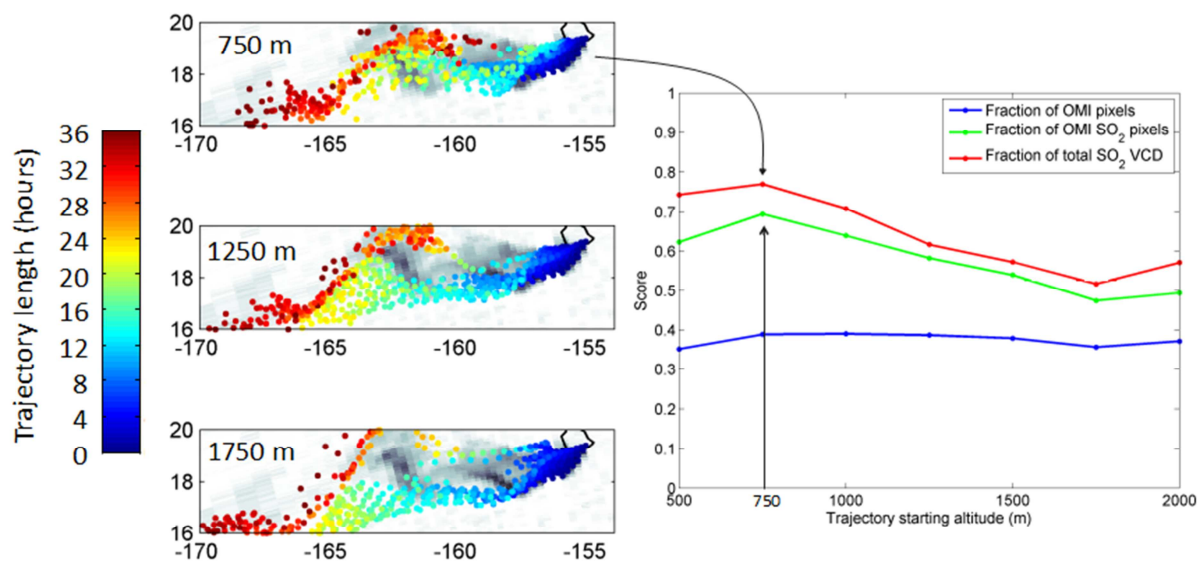


**Figure 2,** Left panels: OMI SO<sub>2</sub> VCD detected on Aug. 7, 2008, at 23 UTC (gray scale) overlaid by all endpoints of forward trajectory calculations started at 0.75, 1.25, or 1.75 km altitude at 20 locations near the volcano at every hour between Aug.7, 22 UTC (OMI overpass time minus 1 hour) to Aug. 6, 11 UTC (OMI overpass time minus 36 hours). Trajectory endpoints are color-coded by their trajectory length.

Right panel: scores for each of seven trajectory sets with starting altitudes between 0.5 and 2.0 km. Blue line, fraction of successful OMI pixels; green, fraction of successful OMI pixels with SO<sub>2</sub> VCD > 1DU; red, fraction of sum of SO<sub>2</sub> VCD of successful pixels. See the text for details.

The best-fitting altitude,  $z_{best}$ , yielded the highest scores and was selected to represent all trajectories belonging to the orbit and was used for further analysis. For the example shown in Fig. 2,  $z_{best}$  = 750 m. Subsequently, SO<sub>2</sub> pixels with their pixel center within a radius of 0.1° from  $z_{best}$ -trajectory endpoints were selected, and their corresponding trajectories were used for further analysis.

Some representative trajectories are shown in Fig. 3 for the orbit on Aug. 7, 2008. Trajectories selected in this manner were used for the cloud history determination. Hourly Level-2 GOES cloud data were evaluated at each step along the trajectory and averaged within a  $0.2^\circ \times 0.2^\circ$  grid box centered at the trajectory point. Geometrical cloud fraction, COT, and cloud top height (CTH) were read out and saved. The latter variable was meant to separate clouds under, within, and above the volcanic plume, but it was found that for the generally low-altitude, optically thin clouds found in the region, the CTH retrieval is rather unreliable. Moreover, we found that clouds in this region generally occur at the same altitude as the volcanic plume, at 1-3 km, hence, it was not surprising that no CTH-dependence was observed. Maps of the  $\text{SO}_2$  data were calculated separately for each cloud-history bin (given by COT thresholds). Similarly, decay traces were calculated by averaging the binned data according to the trajectory length determined for each pixel.

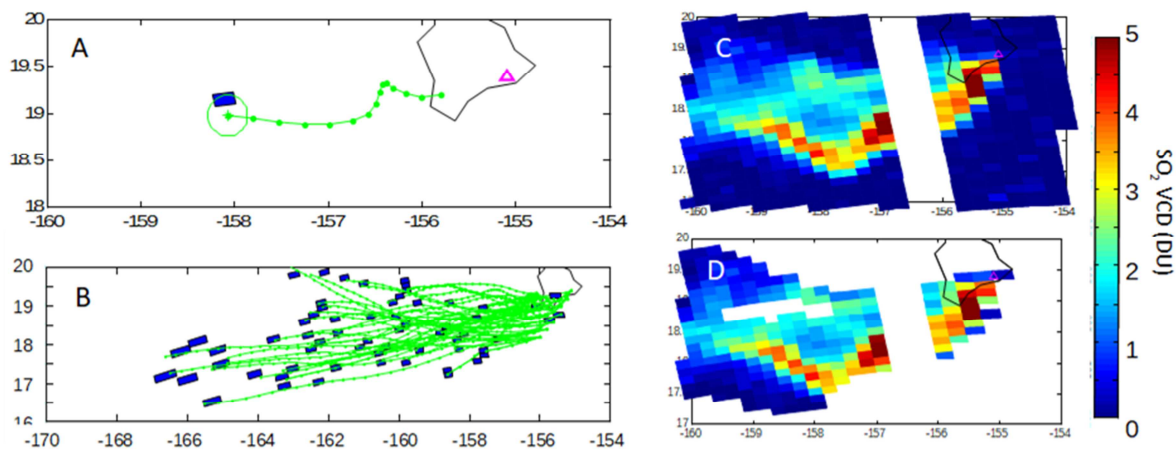


**Figure 3:** Schematic of the forward trajectory method. OMI pixels located within  $0.1^\circ$  of trajectory endpoints were selected. A. Example: OMI pixel measured on Aug. 7, 2008, 23 UTC, trajectory length of 14 hours. B: Pixels (blue) and trajectories (green) for every  $10^{\text{th}}$  successful OMI pixel within this orbit. Note the different longitude scale ( $170^\circ - 154^\circ$  W). C: All OMI  $\text{SO}_2$  VCD within the region (1454 pixels, of which 563 with  $\text{SO}_2 > 0.3$  DU). D: All successful OMI pixels within the region (614 pixels, of which 426 with  $\text{SO}_2 > 0.3$  DU). The rows in the middle of OMI's swath are missing due to the row anomaly.

## 4. RESULTS

The results from our analyses using the forward trajectory method, described in detail above, are shown in Fig. 4. Maps of  $\text{SO}_2$  VCDs, averaged over the time range June-September 2008 (the period of most intensive degassing), and for cumulative COT below and above 50 are shown on the left in the upper and lower panels, respectively. Clear differences in plume shape between the map without cloud interaction (upper) and with (lower) can be seen:  $\text{SO}_2$  columns were generally higher if there were few cloud encounters. However, the expected effect – an increased  $\text{SO}_2$  life time in absence of cloud interactions – was not observed. In addition, the scatter in the data is rather large, despite the averaging of four months' worth of data. This is even more apparent in the decay traces shown on the right of Fig. 4: although the  $\text{SO}_2$  lifetime appears shorter under cloudy conditions (green line), this is due to a single point close to the volcano. Since the region around the volcano is often cloudy, the enhanced VCD is probably an artefact of measurement statistics. Apart from this point at time = 0, the decay traces are identical within their noise range. Similar results were found for the other methods we developed for cloud history determination.

Several things were attempted to improve the results. To remove the initial, probably most error-prone part of the trajectory, the source locations for the forward trajectory method were chosen on a line tangential to the southwestern tip of Hawaii Island. In a different approach, all satellite pixels over the island were discarded before plotting the decay curves. And in stead of using one best-fitting trajectory for every  $\text{SO}_2$  pixel for the determination of cloud statistics, all trajectories that reached that pixel were used and the cloud properties averaged (e.g., the dotted lines in Fig. 4). Source locations and altitudes of the HYSPLIT trajectories were varied, as were the cloud bin thresholds. The algorithms were run

with OMI and GOME-2 data for various time ranges between March and October 2008. And yet, the results refused to become any clearer.

We attribute our inability to capture the cloud effect – at least in part – to the fact that HYSPLIT is not suitable for this specific task. The accuracy of the endpoint’s location required for this analysis, about 10-20 km, is much smaller than the grid size of the used meteorological data set (50 km). In addition, the topography of Hawaii Island cannot be resolved at this grid size and neither can the complex wind movements around the island.

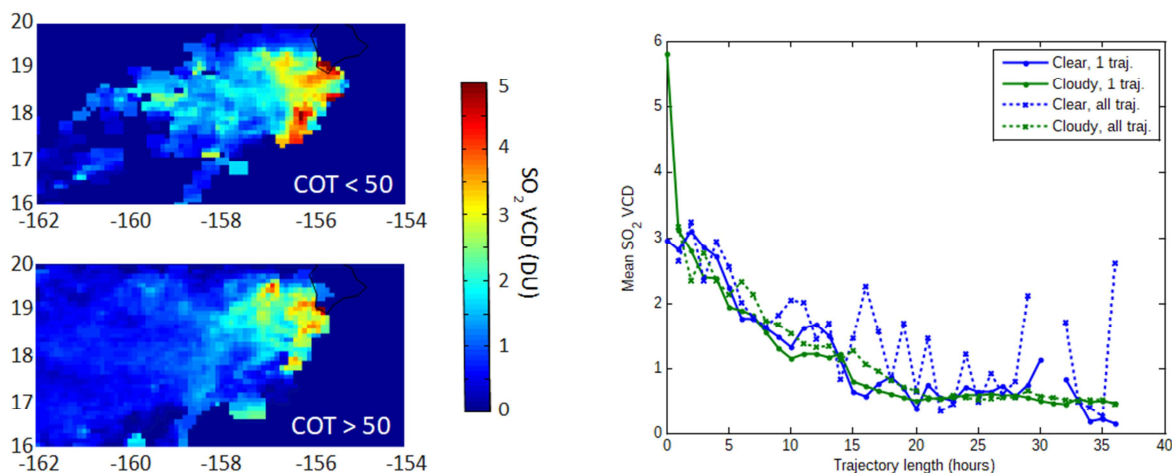


**Figure 4:** Left: Maps of mean SO<sub>2</sub> VCD for June-September 2008, separated by their “cloud history” acquired using the forward trajectory method. Upper panel: data where a total COT < 50 had been encountered. Lower panel: data where clouds with a total COT > 50 were encountered.

Right: SO<sub>2</sub> decay curves of the data shown on the left. Blue lines represent data that encountered a total COT < 50; green lines those with total COT > 50; solid lines indicate the results when a single best trajectory is selected for each satellite pixel, dotted lines use the mean cloud data of all trajectories that reach a pixel.

The methods based on the trajectories of single pixels were then abandoned. We developed other approaches, including: determining mean cloud cover within a certain region (e.g., the mean plume shape observed in August 2008) for a certain time range prior to the satellite overpass and sorting the data orbit-wise. In this fashion, one mean COT was determined for, for example, the 12 hours prior to observation for all pixels within an orbit. The data were subsequently binned by COT and mean SO<sub>2</sub> maps were determined containing data affected by clouds and data without cloud encounters. Yet again, similar results were found as in the previous approaches: there appears to be a difference between clear and cloudy cases, but the normalized decay is very similar for both cases.

Finally, the dependence of the observed SO<sub>2</sub> VCD on cloud properties was investigated systematically. Assuming no chemical effect of clouds on SO<sub>2</sub>, the observed geometrical VCD should only be affected by changes in the light path. Hence for small cloud fraction (CF) the derived geometrical VCD ( $VCD_{obs}$ ) should be very close to the “true” VCD ( $VCD_{true}$ ). For large CF above the volcanic plume, SO<sub>2</sub> is shielded from view and  $VCD_{obs} < VCD_{true}$ ; large CF below the plume cause  $VCD_{obs} > VCD_{true}$ , and large CF within the plume cause observations to be larger or smaller than the “true” value, dependent on COT. In contrast, if in-cloud chemistry causes a faster SO<sub>2</sub> decay, one would expect small values of SO<sub>2</sub> VCD within the cloud, but no effect on SO<sub>2</sub> above or below clouds.

The results are shown in Fig. 5. In the left panels it can be seen that the observed SO<sub>2</sub> VCD increases with CF for clouds below 3 km. Particularly in the region near the volcano (upper left panel) relatively high SO<sub>2</sub> VCD are found at CTH > 2, whereas this is not the case for the outflow region (lower left panel). In the outflow region the largest SO<sub>2</sub> VCD are found for low-lying clouds. One explanation for this is that the volcanic plume has reacted with the clouds near the volcano and the amount of SO<sub>2</sub> has consequently strongly decreased. Another explanation may be a decrease in plume altitude (which would affect the sensitivity of the satellite measurement), although there is no other indication for such plume behavior. It must, however, be pointed out that the statistics for this exercise are not very robust, as apparent from the number of satellite pixels included in each cloud bin, which are shown in Fig.5.

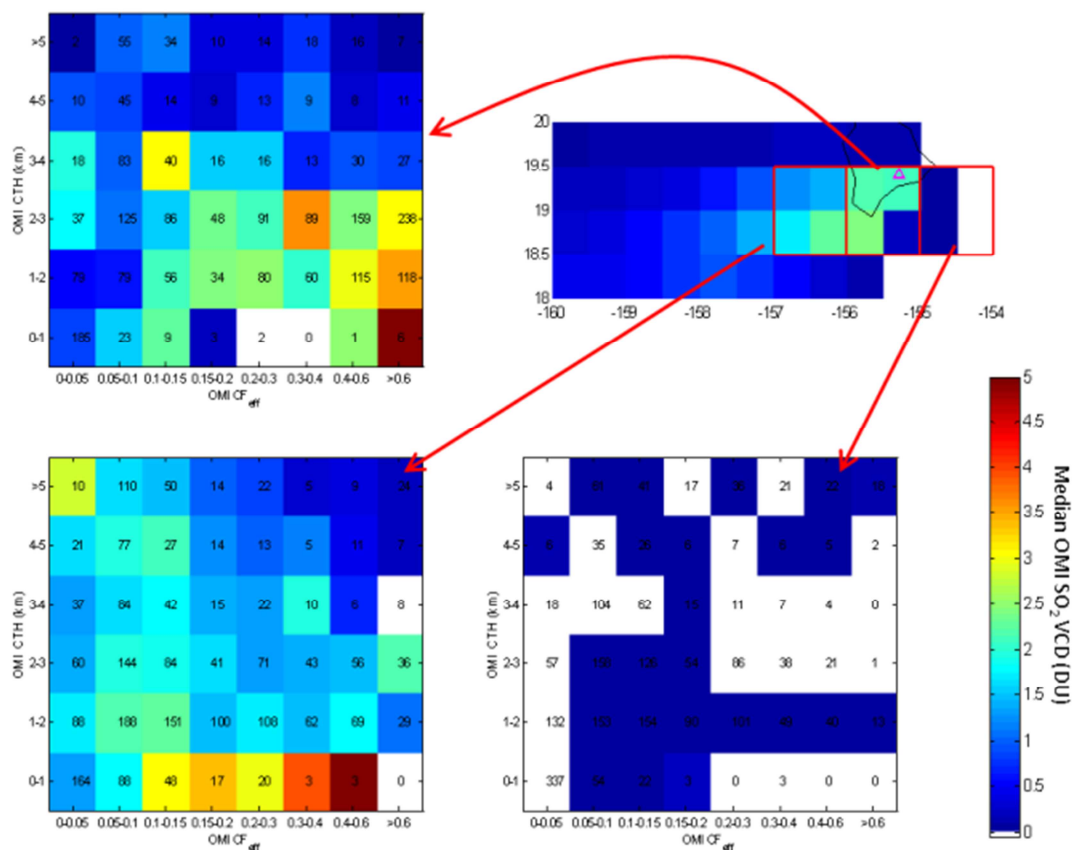


**Figure 5:** Investigation of OMI geometrical SO<sub>2</sub> VCD on cloud properties. Upper right panel: mean SO<sub>2</sub> VCD for May-October 2008. Three remaining panels: median SO<sub>2</sub> VCD binned by OMI effective cloud fraction (CF<sub>eff</sub>) on the x-axis and OMI cloud top height (CTH) on the y-axis for the grid boxes indicated in the upper right panel. Numbers indicate number of pixels included in the analysis.

Shifting the focus from measured to modeled data, we found that the cloud effect on SO<sub>2</sub> is not very pronounced in the modeled data, either. The mean SO<sub>2</sub> VCDs for August 2008 shown in Fig. 6 were calculated using modeled data read out at 23 UTC, the overpass time of OMI. Panels A and B depict the results for the control run and the run with cloud scavenging disabled, respectively. Note that the only difference between the two runs is the cloud scavenging: cloud fields and other meteorological fields are identical. The difference in SO<sub>2</sub> column between the control run and the run in which scavenging of SO<sub>2</sub> was disabled is on the order of  $1 \times 10^{16}$  molec cm<sup>-2</sup> (0.3 DU), a difference that is too small to be resolved using the current set of satellite measurements.

Two possible explanations for the fact that a relatively small difference in SO<sub>2</sub> amount was found when SO<sub>2</sub> scavenging in clouds was switched off are: 1) that the chemistry happens on a scale not resolved by the model, and/or 2) that the amount of clouds is simply too small to yield an observable effect. More conclusive results might have been obtained if the “cloud history” of the modeled SO<sub>2</sub> could have been documented, or reconstructed in some way. For this, a passive tracer would probably have to be used, which was not within the scope of our study.

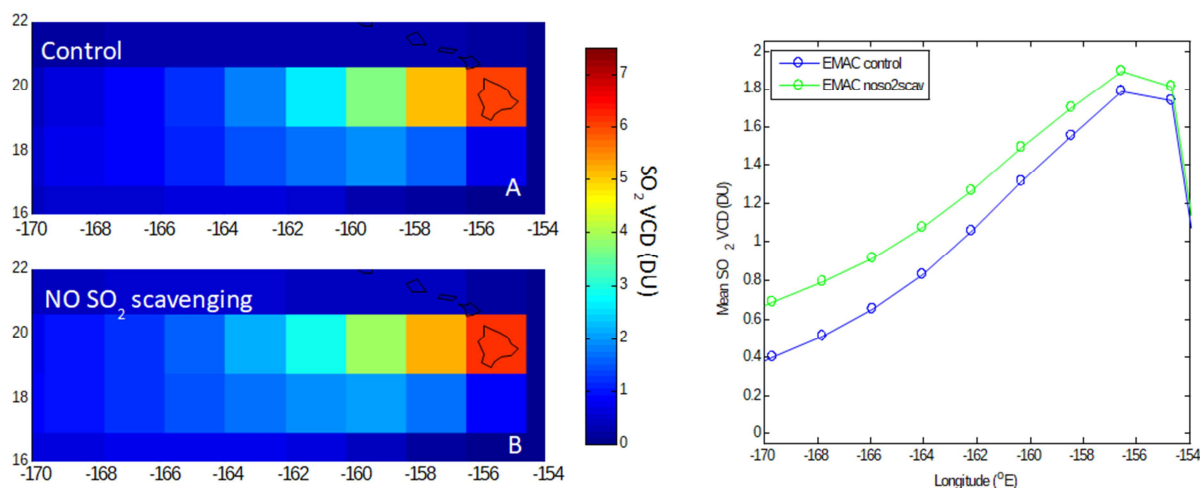


**Figure 6:** Left: mean maps of SO<sub>2</sub> VCD modeled for August 2008 using the EMAC model with SO<sub>2</sub> scavenging switched on (upper) or off (lower). Right panel: SO<sub>2</sub> decay curves for the data shown on the left; control run in blue and the run with SO<sub>2</sub> scavenging switched off in green.

## 5. CONCLUDING REMARKS

Our study has provided many indications that there is an effect of clouds on SO<sub>2</sub> chemistry, but the evidence is not conclusive and neither were we able to quantify it. The main reason for our failure to do so is probably the unsuitability of HYSPLIT as a tool for the required high-precision trajectory determination, particularly near the topographically challenging Hawaii Island. Another important reason is the fact that GOES cloud products are not of sufficient quality in our study area, particularly as the algorithms during day and night are rather inconsistent.

Our systematic study of the dependence of observed SO<sub>2</sub> VCD on cloud properties (COT and CTH) yielded the most promising indications for a chemical cloud effect. In particular, the finding that elevated SO<sub>2</sub> columns were found for CTH > 1 km near the volcano, but not in the outflow region away from the source, is an important – albeit not conclusive – finding.

However, as the elusive cloud effect can apparently not be quantified, we might assume that it may be ignored for the purpose of aerosol model evaluation. In that case, we can simply perform a comparison of model and satellite aerosol data, disregarding any cloud effects. This is the topic of a forthcoming study.

## ACKNOWLEDGMENTS

The free use of cloud data from OMI, GOES, and MODIS instruments, as well as OMI Level-1 data, provided by NASA, is gratefully acknowledged. We are also thankful to NOAA for the HYSPLIT program, which was downloaded from [/www.ready.noaa.gov/HYSPLIT.php](http://www.ready.noaa.gov/HYSPLIT.php)

## REFERENCES

- Beirle, S., Hörmann, C., Penning de Vries, M., Dörner, S., Kern, C. and Wagner, T. (2014) Estimating the volcanic emission rate and atmospheric lifetime of SO<sub>2</sub> from space: a case study for Kilauea volcano, Hawai'i, *Atmos. Chem. Phys.*, **14**, pp. 8309-8322
- Hörmann, C., Sihler, H., Bobrowski, N., Beirle, S., Penning de Vries, M., Platt, U. and Wagner, T. (2013) Systematic investigation of bromine monoxide in volcanic plumes from space by using the GOME-2 instrument, *Atmos. Chem. Phys.*, **13**, pp. 4749-4781

Jöckel, P., Kerkweg, A., Pozzer, A., Sander, R., Tost, H., Riede, H., Baumgaertner, A., Gromov, S. and Kern, B. (2010): Development cycle 2 of the Modular Earth Submodel System (MESSy2), *Geosci. Model Dev.*, **3**, pp. 717-752

Kleist, D. T., Parrish, D. F., Derber, J. C., Treadon, R., Wu, W.-S., Lord, S., Kleist, D. T., Parrish, D. F., Derber, J. C., Treadon, R., Wu, W.-S., and Lord, S. (2009): Introduction of the GSI into the NCEP Global Data Assimilation System, *Weather Forecast.*, **24**, pp. 1691–1705

Minnis, P., Trepte, Q. Z., Sun-Mack, S., Chen, Y., Doelling, D. R., Young, D. F., Spangenberg, D. A., Miller, W. F., Wielicki, B. A., Brown, R. R., Gibson, S. C. and Geier, E. B. (2008): Cloud Detection in Nonpolar Regions for CERES Using TRMM VIRS and Terra and Aqua MODIS Data, *IEEE Trans. Geosci. Remote Sens.*, **46**, pp. 3857-3884

Minnis, P., Sun-Mack, S., Chen, Y., Khaiyer, M. M., Yi, Y., Ayers, J. K., Brown, R. R., Dong, X., Gibson, S. C., Heck, P. W., Lin, B., Nordeen, M. L., Nguyen, L., Palikonda, R., Smith, W. L., Spangenberg, D.A., Trepte, Q. Z. and Xi, B. (2011): CERES Edition-2 Cloud Property Retrievals Using TRMM VIRS and Terra and Aqua MODIS Data; Part II: Examples of Average Results and Comparisons With Other Data, *IEEE Trans. Geosci. Remote Sens.*, **49**, pp. 4401-4430

Pozzer, A., de Meij, A., Yoon, J., Tost, H., Georgoulias, A. K. and Astitha, M. (2015): AOD trends during 2001-2010 from observations and model simulations, *Atmos. Chem. Phys.*, **15**, pp. 5521-5535

Draxler, R. R. and Hess, G. D. (1998): An overview of the HYSPLIT4 modelling system for trajectories, dispersion and deposition, *Aust. Met. Mag.*, **47**, pp. 295–308

Levelt, P. F., van den Oord, G. H. J., Dobber, M. R., Malkki, A., Visser, H., de Vries, J., Stammes, P., Lundell, J. O. V., and Saari, H. (2006): The ozone monitoring instrument, *IEEE Trans. Geosci. Remote Sens.*, **44**, pp. 1093–1101

Stein, A. F., Draxler, R. R., Rolph, G. D., Stunder, B. J. B., Cohen, M. D., and Ngan, F. (2015): NOAA's HYSPLIT Atmospheric Transport and Dispersion Modeling System, *B. Am. Meteorol. Soc.*, **96**, pp. 2059–2077